南京航空航天大学

论 文 集

（二〇〇七年）　第40册

南新院

高　新　院

高新技术研究院2007年发表论文清单

	姓名	职称	单位	论文题目	刊物、会议名称	年、卷、期	类别
1	张助华 郭万林	博士生 正高	高新院纳米所	Magnetic properties of strained carbon nanotubes.	*Appl. Phys. Lett.*	2007. 90, 053114	SCI
2	张助华 郭万林 台国安	博士生 正高 博士生	高新院纳米所	Coaxial nanotubes: carbon nanotubes sheathed with boron nitride nanotubes.	*Appl. Phys. Lett.*	2007. 90, 133103	SCI
3	段晓洁 唐淳 郭万林	博士生 博士生 正高	高新院纳米所	Two distinct buckling modes in carbon nanotube bending	*Nano Letters*	2007. 7: 143-148	SCI
4	郭万林 戴意涛 张斌	正高 博士生 博士生	高新院纳米所	Phase transitions of carbon materials under high pressure	*Iutam Symposium On Mechanical Behavior And Micro-Mechanics Of Nanostructured Materials*	2007. 144: 239-249	SCI
5	郭万林 郭宇峰	正高 中级	高新院纳米所	Energy optimum chiralities of multiwalled carbon nanotubes	*Journal Of American Chemical Society*	2007. 129: 2730-2731	SCI
6	郭宇峰 郭万林	中级 正高	高新院纳米所	Reassembly of single-walled carbon nanotubes into hybrid multilayered nanostructures inside nanotube extruders	*Physical Review B*	2007. 76: 045404	SCI
7	郭宇峰 郭万林	中级 正高	高新院纳米所	Modifying atomic-scale friction between two graphene sheets: A molecular-force-field study	*Physical Review B*	2007. 76: 155429	SCI
8	姜云鹏 郭万林	副高 正高	高新院纳米所	On the study of the effects of notch shape on the creep damage under cyclic loading	*International Journal Of Fatigue*	2007. 29: 836-842	SCI
9	姜云鹏 郭万林	副高 正高	高新院纳米所	On the study of the creep damage development in circumferential notch specimens	*Computational Materials Science*	2007. 38: 653-659	SCI
10	李春 郭万林	博士生 正高	高新院纳米所	First-principles study of the dependence of ground-state structural properties. on the dimensionality and size of ZnO nanostructures	*Physical Review B*	2007. 76: 035322.1-035322.8	SCI
11	李春 郭万林	博士生 正高	高新院纳米所	First-principles study on ZnO nanoclusters with hexagonal prism structures	*Applied Physics Letters*	2007. 90: 223102	SCI
12	李春 郭万林	博士生 正高	高新院纳米所	Size-dependent piezoelectricity in zinc oxide nanofilms from first-principles calculations	*Applied Physics Letters*	2007. 90: 033108	SCI
13	佘崇民 郭万林	初级 正高	高新院纳米所	Three-dimensional stress concentrations at elliptic holes in elastic isotropic plates subjected to tensile stress	*International Journal of Fatigue*	2007. 29: 330-335	SCI/EI
14	佘崇民 郭万林	初级 正高	高新院纳米所	The out-of-plane constraint of mixed-mode cracks in thin elastic plates	*International Journal of Solids and Structures*	2007. 44: 3021-3034	SCI/EI
15	佘崇民 郭万林 孟波 张斌	初级 正高 博士生 博士生	高新院纳米所	椭圆孔三维应力集中及其对疲劳强度的影响	计算力学学报	2007年第2期	
16	台国安 郭万林	博士生 正高	高新院纳米所	Sonochemical preparation of nickel alumina nanotubes templated by anionic surfactant assemblies	*Journal of Materials Science*	2007. 42(24): 10245-10249	SCI
17	台国安 郭万林	博士生 正高	高新院纳米所	Synthesis and characterization of layered and hexagonal nickel-aluminum oxides	*Materials Chemistry and Physics*	2007. 103: 201-205	SCI
18	赵军华 郭万林 佘崇民	博士生 正高 初级	高新院纳米所	The three-parameter description of stress field near the border of an embedded elliptical crack	Acta Mechanica	2007. 190: 29-44	SCI/EI

19	赵军华 郭万林 佘崇民	博士生 正高 初级	高新院纳米所	The in-plane and out-of-plane stress constraint factors and K-T-Tz description of stress field near the border of a quarter-elliptical corner crack	Fatigue and Fracture of Engineering materials and structures	2007. 30: 673-681	SCI/EI
20	赵军华 郭万林 佘崇民	博士生 正高 初级	高新院纳米所	The in-plane and out-of-plane stress constraint factors and K - T - Tz description of stress field near the border of a semi-elliptical surface crack	*International Journal of Fatigue*	2007. 29: 435-443	SCI/EI
21	赵军华 郭万林 孟波	博士生 正高 博士生	高新院纳米所	改进的BP神经网络在多裂纹柱体扭转中的应用	计算力学学报	2007, 24(3):289-293	EI
22	朱纯章 郭万林	博士生 正高	高新院纳米所	An efficient method for evaluating the nanohardness of layer-configured materials by atomistic simulation	Nanotechnology	2007. 18: 295704	SCI
23	刘心声	副高	高新院纳米所	Likelihood ratio test for and against nonlinear inequality constraints	Metrika	2007. 65: 93-108	SCI
24	刘心声 郭万林	副高 正高	高新院纳米所	Robustness of Residue Conservation Score Reflecting both Frequencies and Physicochemistries	Amino Acids	DOI: 10.1007/s00726-007-0017-2	SCI
25	沈启霞 刘心声	硕士生 副高	高新院纳米所	The Monte Carlo EM method for estimating multinomial probit latent variable models	Computational Statistics	DOI 10.1007/s00180-007-0091-7	SCI
26	沈启霞 刘心声	硕士生 副高	高新院纳米所	含缺失数据线性模型回归系数的约束EM算法	南京大学学报：数学半年刊	2007, 24(1): 122-131	核心期刊
27	梁拥成 郭万林	副高 正高	高新院纳米所	过渡金属化合物OsB_2与OsO_2低压缩性的第一性原理计算研究	物理学报	2007年56卷8期4847-4855	核心期刊
28	梁拥成 张英 郭万林 姚裕贵	副高 正高	高新院纳米所	反常霍尔效应理论的研究进展	物理	2007年36卷5期，385-390	核心期刊
29	李海军 郭万林	博士生 正高	高新院纳米所	Casimir力和静电力驱动下同轴圆柱管模型的GHz振动	力学学报	2007年第4期	核心期刊
30	孙升 郭万林	硕士生 正高	高新院纳米所	肌质网钙离子泵蛋白的阳离子亲和性及电势分布	南京航空航天大学第九届研究生学术会议论文集（中图分类号Q615 Q77）	2007	
31	戴振东 孙久荣	正高 正高	高新院仿生所	A biomimetic study of discontinous-constraint metamorphic mechanism for gecko-like robot	Journal of bionic Engineering	2007, 4(2):91-95	
32	戴振东 孙久荣	正高 正高	高新院仿生所	Research progress in gecko locomotion and biomimetic gecko-robot	Progress in Natural Science	2007, 17(1):1-5	
33	戴振东 孙久荣	正高 正高	高新院仿生所	Morphology and contact mechanics influence adhesive characteristics of Dung Beetle'bristle and Gecko's setae	Progress in Natural Science	2007, 17(9):1074-1081	
34	戴振东 张昊 张明 代良全	正高 讲师	高新院仿生所	非连续约束变结构机器人运动机构的仿生：概念及模型	科学通报	2007, 52(1):1-4	核心期刊
35	吉爱红	副高	高新院仿生所	正/零表面上自由运动的黄斑蝽三维接触力测试	传感技术学报	2007. 20. 6	
36	张正杰 吉爱红	硕士 副高	高新院仿生所	用于壁虎脚掌接触力测试的3维传感器	传感技术学报	2007. 20. 6	
37	于敏 沈辉 戴振东	副高 硕士生 正高	高新院仿生所	Manufacture and Performance of Ionic Polymer-Metal Composites	Journal of bionic engineering	2007, 4(3):143-149	
38	赵林林 于敏 戴振东	硕士 副高 正高	高新院仿生所	粗糙聚氨脂表面微接触状态下粘着力的模拟	南京航空航天大学学报	2009. 39. 4	核心期刊

39	倪杰 于敏 沈辉 戴振东	硕士 副高 硕士 正高	高新院仿生所	二维微载荷传感器的设计与分析	传感器与微系统	2007.26.3	
40	汤伊黎 于敏 戴振东 杨松祥	硕士 副高 正高	高新院仿生所	基于多线程技术的运动控制与数据采集程序设计	工业控制计算机	2007.263.3	
41	郭策 王文波 于敏 戴振东	副高 博士 副高 正高	高新院仿生所	大壁虎与无蹼壁虎脚底刚毛结构与其粘附性能的比较研究	中国科学C辑：生命科学	2007.37.5	核心期刊
42	郭策 王文波 于敏 戴振东	副高 博士 副高 正高	高新院仿生所	Comparative studies on the structure and adhesion of setae in G. gecko and G. swinhonis	Science in China series C:Life sciences	2007,50(6):831-838	
43	王文波 郭策 孙久荣 戴振东	博士 副高 正高 正高	高新院仿生所	大壁虎脑立体定位的方法与装置	科学通报	2007.52.21	核心期刊
44	丁红燕 戴振东	博士 正高	高新院仿生所	Sliding friction and wear behavior of TCLL in aqueous condition	wear	2007,(263):117-124	
45	丁红燕 戴振东	博士 正高	高新院仿生所	钛合金在海水中的微动磨损特性	稀有金属材料与工程	2007,36(5):778-781	核心期刊
46	郭东杰	中级	高新院仿生所	Surface-hydrophilic and protein-resistant silicone elastomers prepared by hydrosilylation of vinyl poly(ethylene glycol) on hydrosilanes-poly(dimethylsiloxane) surfaces	Colloids and Surfaces A:Physicochem. Eng. Aspects	2007.308	
47	黄护林 韩东	正高 正高	高新院	Investigation of the performance of the dish/stirling solar thermal electricity system	J. of Energy and Power Eng.	2007.1.1	
48	黄护林 周小明	正高 硕士	高新院	THE IMPACTS OF MAGNETIC FIELDS ON THE THERMOCAPILLARY CONVECTION IN TWO LAYERS FLUID SYSTEM	第5届传热、流体力学及热力学国际会议论文集	2007.5	
49	黄护林 韩东	正高	高新院	EHD对太阳能电推进喷管设计的影响	电推进技术专题研讨会论文集	2007.12	
50	黄护林 方莹	正高 硕士	高新院	MHD Effect on Heat Transfer in Liquid Metal Free Surface Flow around a Cylinder	Engineering Applications of Computational fluid Mechanics	2007.1.2	
51	黄护林 张雪	正高	高新院	磁场对水平温度梯度下双层流体热对流的影响	工程热物理学报	2007.28.S2	核心期刊
52	黄护林 张炎	正高 正高	高新院	磁控等离子体对尾喷管壁传热特性的影响	航空动力学报	2007.22.8	核心期刊
53	周小明 黄护林	硕士 正高	高新院	水平磁场对双层流体热毛细对流的影响	中国工程热物理学会传热传质学术会议论文集	2007.10	
54	张炎 黄护林	正高 正高	高新院	应用磁控等离子体的收缩喷管传热研究	中国工程热物理学会传热传质学术会议论文集	2007.10	
55	王远 王美玲 周飞 丁红燕	硕士 副高 正高 副高	高新院	不同环境条件下铝合金微弧氧化陶瓷膜的摩擦磨损性能	中国有色金属学报	2007.17.8	核心期刊
56	周飞 王远 刘峰 孟月东	正高 硕士	高新院	铝合金表面Al2O3薄膜及Al2O3/CrN多层薄膜在水中的摩擦磨损性能的研究	2007年全国第八届摩擦学会议	2007.17.8	
57	周飞 王晓雷 加藤康司 戴振东	正高 正高	高新院	Friction and wear property of a-CNx coatings sliding against Si3N4 balls in water	Wear	2007.263.7-12	

58	刘兴华 曹云峰 沈春林	博士生 研究员 教授	高新院	基于对应线标定的无人机着陆位姿确定算法	传感器与微系统	2007年26卷9期	核心期刊
59	梅羡林 曹云峰 庄丽葵 黄护林	硕士 研究员 工程师 教授	高新院	the design of flight control system for mini uav	ICIUS 2007	2007	国际会议
60	丁萌 曹云峰 吴庆宪 张珍	博士生 研究员 教授 硕士	高新院	image processing in optical guidance for autonomous landing of lunar probe	ICIUS 2007	2007	国际会议
61	丁萌 曹云峰	博士生 研究员	高新院	利用计算机视觉获取无人机飞行姿态角	传感器与微系统	2007年26卷11期	核心期刊
62	郭琳 曹云峰	硕士 研究员	高新院	旋翼模型操纵系统设计与实现	计算机测量与控制	2007年15卷8期	
63	唐磊 曹云峰	硕士 研究员	高新院	微型飞行器的飞行试验	航空兵器	2007年第4期	
64	唐磊 曹云峰	硕士 研究员	高新院	某型MAV的自主导航算法及飞行试验	指挥控制与仿真	2007年29卷4期	
65	唐翠娥	中级	高新院	大力推进高校校园文化建设	教育前沿	2007.5	
66	唐翠娥	中级	高新院	对完善工会财务工作的思考	集团经济研究	2007.7	
67	唐翠娥	中级	高新院	高效科研团队建设的人力资源研究	集团经济研究	2007.11	
68	朱旭东	初级	高新院	浅谈新形势下的高校科研管理	中国科技信息	2007.20	
69	朱旭东	初级	高新院	新形势下高校科技保密工作研究	中国科技信息	2008.1	

Magnetic properties of strained single-walled carbon nanotubes

Zhuhua Zhang and Wanlin Guo[a]

Institute of Nano Science, Nanjing University of Aeronautics and Astronautics, Nanjing 210016, People's Republic of China

Strong effects of uniaxial and torsional strains on the magnetic properties of single-walled carbon nanotubes have been investigated by tight binding calculations and the Green function analyses. The strain-induced peaks of susceptibility are found in the carbon nanotubes, and paramagnetic-diamagnetic transition takes place at certain strains. The critical magnetic flux for semiconductor-metal transition changes linearly with strains depending on the chiralities of the tubes, mainly due to the tuning of the Van Hove singularities by the coupling of strains and magnetic flux. The positive and negative strain effects are asymmetrical in chiral tubes. © 2007 American Institute of Physics. [DOI: 10.1063/1.2450644]

A single-walled carbon nanotube (SWCNT) exhibits either metallic or semiconducting character depending on its chirality and diameter.[1] The electronic structure of a SWCNT can be significantly tuned by mechanical strains, presenting a strong electromechanical coupling.[2–5] This coupling effect has been confirmed by many experiments in the SWCNTs, which has potential applications in nanodevices.[6,7] Recently, more and more theoretical and experimental researches showed that the SWCNTs have abundant magnetic properties as well,[8,9] and a periodic Aharonov-Bohm oscillations in the conductivity of the SWCNT and large diamagnetic susceptibilities have been observed when a magnetic field is applied parallel to the tube axis.[10–13] However, the particular physics of electronic states coupled to both strains and magnetic field, and magnetic responses to mechanical deformation remain to be quantified in SWCNTs theoretically.

In this letter, the electronic variations of SWCNTs under the coupled effects of the uniform deformation and an axis-oriented magnetic field are studied systematically based on a π-orbital tight binding (TB) theory. We found that strains can lead to significant change in susceptibility as well as strain-induced paramagnetism—diamagnetism transition for almost all types of SWCNTs. A linear relationship between the critical magnetic flux and strain is exhibited, which shows chirality-dependent asymmetry caused by positive and negative strains.

In all the following expressions, the superscript 0 is used to denote the undeformed states without special statement, and the physical quantities are described in a chirality dependent (c,t) coordinate system, which consists of the circumferential component c and its perpendicular t in the SWCNT. In a strained SWCNT, the C–C bond will be stretched or compressed. The deformed space vectors are $\mathbf{r}=\mathbf{r}^0+\Delta\mathbf{r} = \mathbf{r}^0(I+\xi)$, where I and ξ represent the unit matrix and a two—dimensional strain tensor, respectively. The effect of strains enters the TB Hamiltonian matrix element via $H_j(\mathbf{k},\xi)=H_j^0(\mathbf{k})\tau_j(\exp i\mathbf{k}\cdot\Delta\mathbf{r}_j)$, where $\tau_j=(r_j^0/r_j)^2$ is a factor from the Harrison hopping relationship,[14] and $j=1,2,3$ label the three bonds from a carbon atom with bond length r_j and vector $\mathbf{r}_j=\mathbf{r}_j^0+\xi\mathbf{r}_j^0$. This disposal to the Hamiltonian has been employed to rightly predict the electronic structures of de-

formed SWCNTs near Fermi level.[4,15] Here, we extend the approach to SWCNTs under an axis-oriented magnetic field. In this case, the Hamiltonian should be modified by a phase factor,

$$H_j(\mathbf{k},\xi,\phi)$$
$$= H_j^0(\mathbf{k})\tau_j(\exp i\mathbf{k}\cdot\Delta\mathbf{r}_j)\exp\left[i(2\pi/\phi_0)\int_{\mathbf{r}_j}\mathbf{A}\cdot d\mathbf{r}\right], \quad (1)$$

where ϕ denotes the magnetic flux threading the SWCNT, ϕ_0 is the flux quantum, and $\mathbf{A}$ denotes the vector potential,[16] which is a function of strain and magnetic flux. It should be pointed out that Harrison's formula is usually valid in the case of small strain of the bond length, which is accurate enough in our calculated strain range within 6%, as large deformation can destroy the SWNT.[17] The hybridization of σ and π orbits induced by curvature effect can cause a modification in the energy gap of the SWCNT.[2] However, this modification varies as the inverse square of the SWCNT radius,[2,18] which can be neglected in our model when considering relatively large SWCNTs. In fact, curvature changes induced by tensile and torsional strain are higher order small values. From the Hamiltonian matrix, the energy dispersion can be obtained as

$$E(k_c,k_t,\varepsilon_t,\gamma,\phi) = \{V_1^2 + V_2^2 + V_3^2 + 2V_1V_2\cos\omega_1$$
$$+ 2V_2V_3\cos\omega_2 + 2V_1V_3\cos(\omega_1+\omega_2)\},$$

$$\omega_1 = k_c(r_{1c}-r_{2c}) + k_t(r_{1t}-r_{2t}) + 2\phi(r_{1c}-r_{2c})/D\phi_0,$$

$$\omega_2 = k_c(r_{2c}-r_{3c}) + k_t(r_{2t}-r_{3t}) + 2\phi(r_{2c}-r_{3c})/D\phi_0, \quad (2)$$

where $V_j=V^0\tau_j$ denote the transfer integrals of the strained SWCNT with $V^0=2.66$ eV, ε_t is the uniaxial strain, γ is the torsion strain, and D represents the diameter of the SWCNT. Here the electronic states are restricted to the allowed states by the boundary condition $\pi Dk_c=2\pi q$, with q an integer.

The density of states (DOS) of the π electron in a SWCNT can be given by the imaginary part of the diagonal Green function.[15] Under the coupled effects of the magnetic flux and strains, the diagonal Green function can be written as

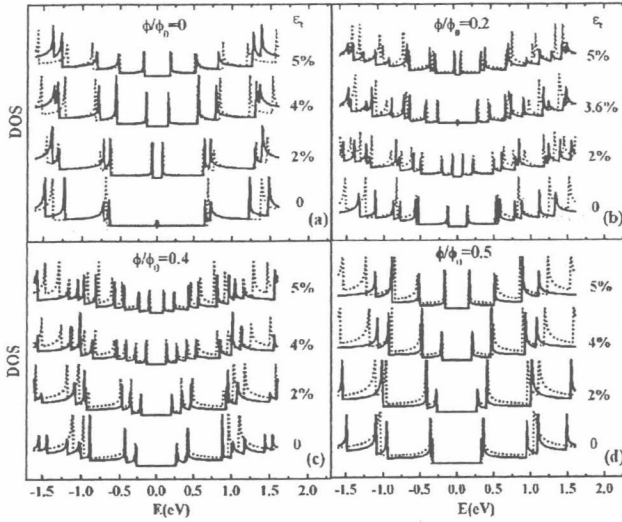[a]Electronic mail: wlguo@nuaa.edu.cn

FIG. 1. DOS near the Fermi level of a (21, 0) SWCNT at different fluxes obtained from the method of Green's function (solid lines) and the theory from Ref. 19 (dot lines). Values on the right side are stretching strains, and the energy interval between the lowest VHS positions is the gap.
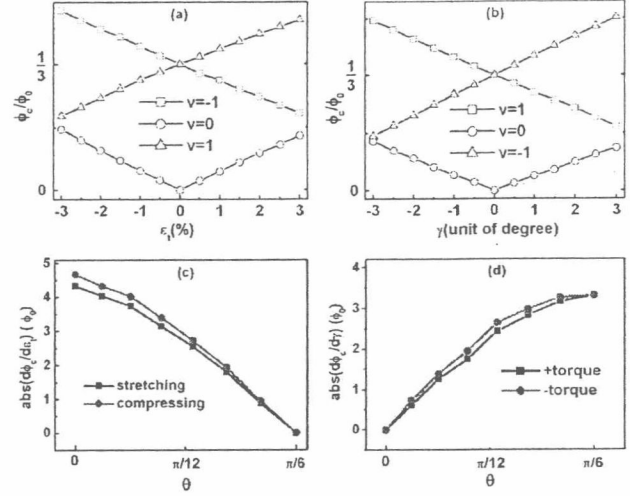

FIG. 2. Critical flux for semiconductor-metal transition as functions of strains and the asymmetrical effects caused by negative and positive strains. The slopes of the critical magnetic flux vs strain as functions of the chirality angle θ for SWCNTs (n,m) with $n+m=14$. (a) and (c) show the case of uniaxial strain, while (c) and (d) represent the case of torsion (>0 for net bond stretching and <0 for net bond compression). The "abs" represents the absolute value, and $v=(n-m)\mathrm{mod}\,3$.

$$G(\omega + i\varsigma)$$

$$= \frac{\Omega}{2\pi N} \lim_{\varsigma \to 0^+} \sum_q \int_{k_t} \frac{\omega + i\varsigma}{(\omega + i\varsigma)^2 - E(q,k_t,\varepsilon_t,\gamma,\phi)^2} dk_t, \quad (3)$$

where Ω is the volume of the (one dimensional) unit cell, N is the number of unit cell in the tube, and ω is the energy. The total DOS ρ is given by the negative imaginary part of the Green function,

$$\rho(\omega) = -\mathrm{Im}[G(\omega)]. \quad (4)$$

To verify the method discussed above, we have also calculated the coupled effects on the DOS of SWCNTs of arbitrary chiralities and diameters under various strains and magnitudes of magnetic field by using the theory from Ref. 19, which makes an assumption about the energy bands being linear near the Fermi level so that it can only reflect the electronic structures near the Fermi level. In Fig. 1, we plot the DOS of the (21, 0) SWCNT under the coupled effects of flux and stretching deformation. A good coincidence is found between the two methods at lower strains and lower energies. Similar results can be obtained for other types of SWCNTs as well.

For the (21, 0) SWCNT under stretching only, the Van Hove singularities (VHSs) split first, then shift and merge with increasing strain, resulting in a metal-semiconductor transition, as shown in Fig. 1(a). For the strained SWCNT, when threaded by ϕ, splitting of VHS occurs again, and the coupled effects of different values of strain and flux make the VHSs shift and merge slower or faster, so that the field-induced metal-semiconductor transition in the tube can be modulated into other transition modes by strain (Fig. 1), such as a semiconductor-metal-semiconductor transition. If the magnetic flux is withdrawn, our results can meet the findings of Ref. 4.

Now, concretely, the effects of strains on the critical magnetic flux (labeled as ϕ_c, which induces semiconductor-metal transition) will be discussed. Under the strains within the above discussed range, it can be clearly seen that the ϕ_c changes linearly with strains [Figs. 2(a) and 2(b)], and the

sign and the slope of $d\phi_c/d\varepsilon_t$ (or $d\phi_c/d\gamma$) depend on the chirality and chirality angle of the SWCNT, respectively. For a set of SWCNTs (n,m) with $n+m=14$, the effects of the chirality angle on the absolute values of $d\phi_c/d\varepsilon_t$ and $d\phi_c/d\gamma$ are shown in Figs. 2(c) and 2(d), respectively. It is shown that the uniaxial strain is more sensitive for SWCNTs with smaller chirality angle, while the torsion strain shows a contrary character. We can see that the uniaxial/torsional strain can hardly modulate the critical magnetic flux of armchair/zigzag SWCNTs, but can easily modulate that of zigzag/armchair SWCNTs. It is interesting to find that positive and negative strains have asymmetrical effects on the critical magnetic flux of chiral SWCNTs. The asymmetrical effects are relative with the asymmetrical structures of the chiral SWCNTs. For example, the armchair tube, due to its pure symmetry, always shows symmetrical change with positive and negative strains, but this is limited to small strain.[20] Under an applied strain, convenient modulation of the critical flux by strains suggests that only a relatively weaker field is adequate to realize the semiconductor-metal transition. If the strain is set to zero, our calculations can reproduce that of Ref. 12.

The strong strain-dependent magnetic response in the SWCNT implies a strain-related magnetic susceptibility. The total susceptibility χ contains two contributions, the spin term χ_s and the orbital term χ_{orb}. We neglect χ_s and let $\chi = \chi_{orb}$ according to Lu's research.[12] For the strained SWCNT, χ can be deduced from the free energy,[12,21]

$$\chi(T) = \left(-\pi^2 R^4 \frac{\partial^2 F(\phi,T)}{\partial \phi^2} \right)_{\phi=0}, \quad (5)$$

where $F(\phi,T) = -k_B T \sum_{q,k_t} \ln(1 + \exp[E_q(q,k_t,\varepsilon_t,\gamma,\phi) - \mu)/k_B T])$ is the free energy of the SWCNT at temperature T, and μ denotes the chemical potential.

The susceptibility of carbon nanotubes is anisotropic and changes according to the orientation of the applied magnetic
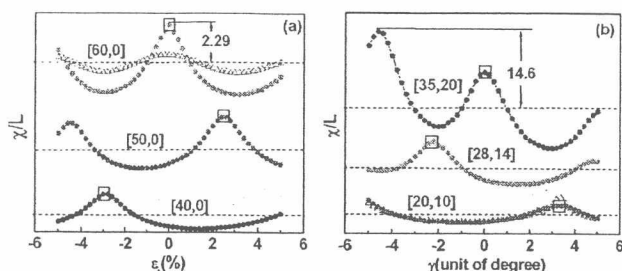
FIG. 3. Susceptibility per nanometer of the strained SWCNTs and the susceptibility peak caused by the strains. (a) The effects of uniaxial strain on the susceptibility of three types of SWCNTs at temperature of 0 K, where triangles represent the case of (60, 0) SWCNT at temperature of 600 K for comparison. (b) The effects of torsion on the susceptibility at temperature of 300 K, where triangles exhibit the case of (20, 10) SWCNT at temperature of 0 K. $\mu=0$ eV. The first peak of each curve is denoted by a square. The dot lines denote the value of zero susceptibility, and the numbers which denote the peak values are in unit of 10^{-5} cgs/(mole nm).

field.[11,12] Here, we only discuss the case of axis-oriented magnetic flux. However, in this case, the behavior of the susceptibility of the strained SWCNTs is diversified and full of surprises, as shown in Fig. 3. In the absence of strains, it is shown that the SWCNTs with $\nu=0$ are paramagnetic and the SWCNTs with $\nu=\pm1$ are diamagnetic, as can be expected by the previous studies.[12] In the presence of strains, however, the susceptibility shows a surprising oscillation with strains, whose breadth and amplitude depend on the chirality and the diameter of the SWCNT. For each SWCNT, the peak nearest to the zero point of strain is labeled as the first peak (denoted by a square in Fig. 3). The position of the first peak depends on the tube chirality and the strain mode, which can be concluded from Fig. 3. Our extensive calculations also show that (1) for SWCNTs with given chirality angle, the distance between two proximate peaks decreases with increasing diameter, following an increase in the peak value; (2) for SWCNTs with identical diameter, within the same strain range, the number of the peaks decreases with increasing chirality angle in the case of uniaxial strain, but increases in the case of torsion strain. There is an exception that the susceptibility curve of an armchair SWCNT versus uniaxial strain has the largest number of peaks, mainly due to its immunity to uniaxial strain. We must stress that the effect of temperature is mainly connected with the roughness of the χ-strain curves, which shows that the higher temperature, the smoother curves.

The underlying reason of the oscillation of susceptibility should be placed on the strain-induced semiconductor-metal transition in SWCNTs. If a SWCNT is a semiconductor initially, it would possess a diamagnetic susceptibility. However, its band gap decreases gradually with strain, leading to the increase in the susceptibility and a diamagnetism-paramagnetism transition, and when the gap disappears, the susceptibility will achieve the peak value. For chiral SWCNTs as shown in Fig. 4(b), the peak value of susceptibility increases along the negative direction of the strain axis, which suggests that chiral tubes can always possess a paramagnetic susceptibility under enough large negative torsion (for net bond compression): this character is unique to the chiral tubes under torsion. The oscillation of the susceptibility with strain reflects the strain-induced periodic metal-semiconductor transition character in SWCNTs. As the susceptibility can be modulated by strains so significantly, we

can expect that a giant diamagnetic or paramagnetic susceptibility can be obtained conveniently in any SWCNTs by applying strains. More importantly, the switching of the sign of susceptibility implies a strain-induced diamagnetism-paramagnetism transition when the strain reaches a critical value (except for the armchair tubes). New nanodevices may be designed using this transition mechanism, such as a nanoswitch for magnetization.

In conclusion, our TB analyses show that the magnetic properties of SWCNTs can be significantly tuned by strains. The critical magnetic flux for semiconductor-metal transition has a linear but chirality-dependent relationship with strains. The chirality-related asymmetry is found from the effects of positive and negative strains on the transition. Furthermore, the susceptibility of strained SWCNTs has strain-induced peaks, whose values and distributions rely on both the chirality and the diameter of the SWCNTs. A switch between paramagnetism and diamagnetism is found at certain strains. Some factors such as spin-magnetic field interaction may affect the magnetic properties of the SWCNTs and deserve further studies.

[1] J. W. Mintimire, B. I. Dunlap, and C. T. White, Phys. Rev. Lett. 68, 631 (1992); Jeroen W. G. Wildoer and L. C. Venema, Nature (London) 391, 59 (1998); T. W. Odom and J. L. Huang, ibid. 391, 61 (1998).

[2] C. L. Kane and E. J. Mele, Phys. Rev. Lett. 78, 1932 (1997).

[3] L. F. Chibotaru, S. A. Bovin, and A. Ceulemans, Phys. Rev. B 66, 161401(R) (2002); W. Guo and Y. Guo, Phys. Rev. Lett. 91, 115501 (2003).

[4] L. Yang and J. Han, Phys. Rev. Lett. 85, 154 (2000).

[5] J. Q. Lu, J. Wu, and W. H. Duan, Phys. Rev. Lett. 90, 156601 (2003); Bin Shan, G. W. Lakatos, and S. Peng, Appl. Phys. Lett. 87, 173109 (2005).

[6] J. Cao, Q. Wang, and H. J. Dai, Phys. Rev. Lett. 90, 157601 (2003); E. D. Minot, Y. Yaish, and V. Sazonova, ibid. 90, 156401 (2003); L. J. Li, R. J. Nicholas, R. S. Deacon, and P. A. Shields, ibid. 93, 156104 (2004); A. Maiti, A. Svizhenko, and M. P. Anantram, ibid. 88, 126805 (2002).

[7] S. Paulson, M. R. Falvo, and N. Snider, Appl. Phys. Lett. 75, 2936 (1999).

[8] J. Jiang, J. Dong, and D. Y. Xing, Appl. Phys. Lett. 83, 5515 (2003); H. Ajiki and T. Ando, J. Phys. Soc. Jpn. 62, 1255 (1993).

[9] E. D. Minot, Y. Yaish, V. Sazonova, and P. McEuen, Nature (London) 428, 536 (2004); U. C. Coskun, T. C. Wei, and S. Vishveswara, Science 304, 1132 (2004); S. Zaric, G. N. Ostojic, and J. Kono, ibid. 304, 1129 (2004).

[10] J. O. Lee, J. R. Kim, J. J. Kim, J. Kim, and N. Kim, Solid State Commun. 115, 467 (2000); A. Fujiwara, K. Tomiyama, and H. Suematsu, Phys. Rev. B 60, 13492 (1999).

[11] F. Tsui, L. Jin, and O. Zhou, Appl. Phys. Lett. 76, 1452 (2000).

[12] J. P. Lu, Phys. Rev. Lett. 74, 1123 (1995).

[13] A. P. Ramirez, R. C. Haddon, O. Zhou, R. M. Fleming, J. Zhang, S. M. McClure, and R. E. Smalley, Science 265, 84 (1994).

[14] W. A. Harrison, Electronic Structure and the Properties of Solids: The Physics of the Chemical Bond (Freeman, San Francisco, 1990).

[15] R. Heyd, A. Charlier, and E. McRae, Phys. Rev. B 55, 6820 (1997).

[16] T. B. Boykin, R. C. Bowen, and G. Klimeck, Phys. Rev. B 63, 245314 (2001).

[17] M. F. Yu, B. S. Files, S. Arepalli, and R. S. Ruoff, Phys. Rev. Lett. 84, 5552 (2000).

[18] X. Blase, L. X. Benedict, E. L. Shirley, and S. G. Louie, Phys. Rev. Lett. 82, 1225 (1994).

[19] J. W. Mintmire and C. T. White, Phys. Rev. Lett. 81, 2506 (1998).

[20] T. Ozaki, Y. Iwasa, and T. Mitani, Phys. Rev. Lett. 84, 1712 (2000).

[21] M. Marganska, M. Szopa, and E. Zipper, Acta Phys. Pol. A 106, 609 (2004).

Coaxial nanocable: Carbon nanotube core sheathed with boron nitride nanotube

Zhuhua Zhang, Wanlin Guo,[a) and Guo'an Tai
Institute of Nano Science, Nanjing University of Aeronautics and Astronautics, Nanjing 210016, China

A coaxial nanocable model consisting of conductive carbon nanotube core and boron nitride nanotube sheath is proposed by *ab initio* calculations. The conduction electron density is mainly concentrated on the inner carbon shell at the optimal interwall distance about 0.35 nm. The conductivity of the core carbon nanotube and the insulation of the boron nitride nanotube sheath are found to be rather tolerant to mechanical deformation. © *2007 American Institute of Physics.*
[DOI: 10.1063/1.2714997]

As the development of nanoelectromechanical systems (NEMSs),[1] excellent interconnections for nanoscale electronic elements have been considered widely. Suenaga *et al.*[2] synthesized a sandwich structure made of carbon layers and boron nitride (BN) layers, which resembles the structure of nanocable but cannot present the function. A coaxial nanocable consisting of SiC/SiO_2 sheathed with BN and carbon was prepared by Zhang *et al.*[3] Subsequently, many coaxial structures have been synthesized, such as $B-SiO_2$,[4] $SiC-SiO_2$,[5] $Zn-ZnS$,[6] TiO_2-SiO_2,[7] and $Ag-C$,[8] but few of them can act as a nanocable for the weak electrical capability. Recently, Zhou *et al.*[9] proposed a theoretical nanocable model of copper nanowires encapsulated in BN nanotubes (BNNTs), where the BNNTs could function as insulating sheaths excellently. However, an ideal nanocable should own light weight for suspending in NEMS and, importantly, high strength to resist the mechanical deformation. Carbon nanotubes (CNTs) with excellent mechanical,[10] electrical,[11] and magnetic[12] properties have been regarded as an important component in future devices. On the other hand, the BNNTs exhibit high strength, thermal stability, and chemical inertness, especially insulators regardless of their chirality and diameters.[13] Multiwalled BNNTs have been also reported and found that the majority of them are even walled.[14] Recently, both experiments and theoretical calculations have shown that nanopeapods formed by encapsulating of C_{60} into BNNTs could exist stably,[15,16] which may provide an effective material to prepare a coaxial structure composed of inner CNT and outer BNNT under appropriate conditions.

In this work, coaxial nanocables consisting of conductive CNT core and insulating BNNT sheath are investigated by *ab initio* calculations. We find that the interwall distance in the most favorable nanocables is about 0.35 nm. The interwall interaction between CNTs and BNNTs is extremely weak and the conduction electrons are mainly concentrated on the CNTs. Contrary to other nanocables, the present model can sustain a high conductivity even under large mechanical deformation.

All calculations have been performed using ultrasoft pseudopotentials with a plane-wave basis.[17] In our calculations, one-dimensional periodic boundary condition is applied along the nanotube axis with multiple k sampling. One

unit cell of the nanocable along the axis is included in our calculations and the distance between two nearest nanocables is about 0.8 nm. All the atoms in the unit cell are fully relaxed until the force on each atom is less than 0.1 eV/nm.

Interwall interaction energies are calculated for achiral configuration of the proposed nanocable, which are defined as the energy difference between the total energy of the combined system and the summation of the total energies of an isolated CNT and a pristine BNNT in the same simulation box, calculated with the same parameters. We take armchair configuration (5,5)-(n,n) ($n=8-12$) and zigzag (6,0)-$(m,0)$ ($m=13-17$) to clarify the energetics of the nanocables consisting of thin CNTs and thick BNNTs, as shown in Fig. 1. It is found that the (10, 10) and (15, 0) outer BNNTs are the most energetically favorable for the inner (5, 5) and (6, 0) CNTs, respectively. Both of them imply an optimal interwall distance of about 0.35 nm. However, there may be some other chirality configuration of the proposed nanocable, such as chiral-chiral and chiral-zigzag, but the nature of the interwall interaction is nearly identical and is not the focus of this study. For simplicity, we have considered only the armchair configuration with armchair-armchair in the proposed nanocable.
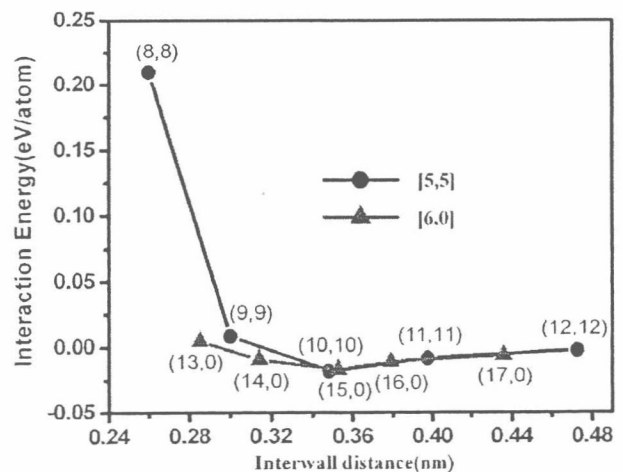

FIG. 1. (Color online) For a selected inner CNT core, total energy per atom of each nanocable as a function of the interwall distance between the inner CNT and the outer BNNT. Circles and triangles denote the case of (5,5)-(n,n) and (6,0)-$(m,0)$ nanocables, respectively.

[a)]Author to whom correspondence should be addressed; Fax: +86 25 84895827; electronic mail: wlguo@nuaa.edu.cn
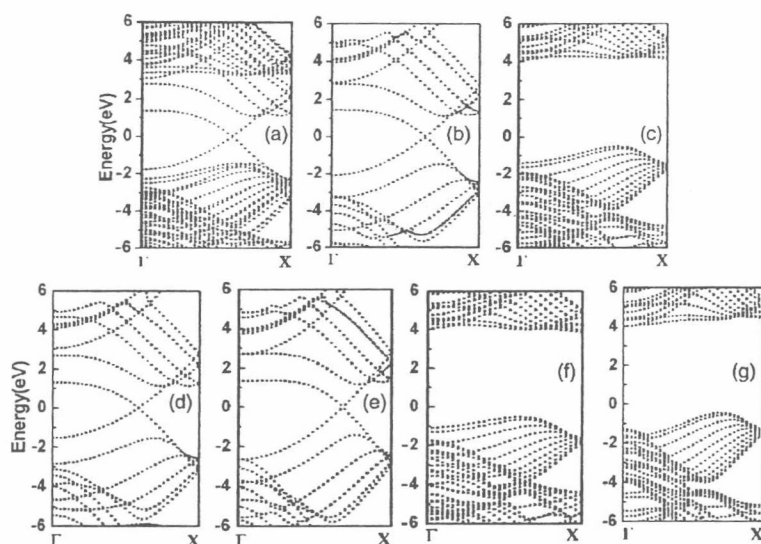
FIG. 2. Band structures of (a) (5, 5)-(10, 10) nanocable, (b) (5, 5) CNT, and (c) (10, 10) BNNT. The electronic structures of (5, 5) CNT under axial strains for (d) stretching 5% and (e) compressing 5% are shown for comparison. (f) and (g) exhibit the electronic bands of (10, 10) BNNT under axial strains for stretching 5% and compressing 5%, respectively. The Fermi level is located at 0 eV.

To investigate the interwall interaction between the outer BNNTs and the inner CNTs, the electronic structure of (5, 5)-(10, 10) is calculated, as shown in Fig. 2(a). The band structures of the individual CNT and BNNT are also shown in Figs. 2(b) and 2(c) for comparison, respectively. A wide energy gap of about 4.4 eV near the Fermi level is found with (10, 10) BNNT (the gap is in good agreement with previous *ab initio*[18] and tight-binding[13] results), while the (5, 5) CNT exhibits a metallic nature. From Fig. 2(a), a simple superposition of the band structures of the individual BNNT and CNT can be found clearly. However, there is a small variation of the electronic structure of the CNT when compared with that of the pristine CNT and also for BNNT. The variations are due to the small difference between the bond lengths of C–C and B–N, which makes the C–C bond stretched and the B–N bond compressed a little in our computed unit cell model for matching the periodic boundary condition. To show the effect of axial deformation, we also performed calculations for band structures of individual BNNTs and CNTs under uniaxial strain of ±5%, which are shown in Figs. 2(d)–2(g). It is found that the sheath BNNT and the core CNT always keep insulating and conductive, respectively. The small variations of the bottom of conduction band and the top of valence band at the Γ are worthy of attention, which indeed imply that the C–C bonds are stretched and B–N bond are compressed slightly in the unit cell. This disposal to the unit cell hardly affects the weak interaction between the sheath and the core of the nanocable.

The transport properties of the nanocable can be further evaluated by computation of the partial electron density on the two bands crossing the Fermi level. In the left panel of Fig. 3, we plot the charge density of the conduction electrons, which indicates that the conductive electrons are mainly distributed on the inner CNT but seldom on the outer BNNT shell. The isosurface for the charge density discussed above, as shown in the right panel of Fig. 3, further indicates that the outer BNNT cannot participate in the electron transport. Therefore, the electronic current is only carried by the inner CNT, while the outer BNNT acts well as an insulating sheath simultaneously.

We also studied the electronic behavior of the squashed (5, 5)-(10, 10) nanocable, as shown in Fig. 4. Similar to Ref. 19, two identical tips are used to squash the nanocable with a

width of $w=0.15$ nm symmetrically about its center. The squashed nanocable structures are optimized at each tip position. In Fig. 4(a), the variation of energy gap of the nanocable with distance between the two tips [labeled by d in Fig. 4(a)] is drawn. When $d>0.93$ nm, it is found that the gap opening is less than 0.02 eV, which is mainly because the inner CNT is squashed into a elliptical shape by the outer BNNT and the atoms at the top and bottom sides of the CNT interact weakly (a weak π-π^* interaction). But when 0.59 nm $<d<0.93$ nm, the gap opens up to nearly 0.2 eV and the nanocable becomes a semiconductor as the atoms at the top and bottom sides of the inner CNT start to form sp^3-type bonds (a strong π-π^* interaction). Besides, the curvature at the edges of the CNT would lead to a strong π-σ interaction and partial transfer of charge to the curvature region [Fig. 4(c)], which can raise the σ bands, so that the gap opening may be canceled a little in this case.[20] However, the gap closing at $d<0.59$ nm should be attributed to the interaction between the outer BNNT and the inner CNT. From Fig. 4(d), it can be clearly seen that dangling bonds have been formed between the BNNT and CNT, and the conduction electrons have been transferred partially into the outer BNNT. Thus, at this point, the nanocable has been ruined. In order to further understand the gap closing, the band structure of the nanocable at $d=0.55$ nm is plotted in Fig. 4(b), where the π bands of the inner CNT are flattened by the
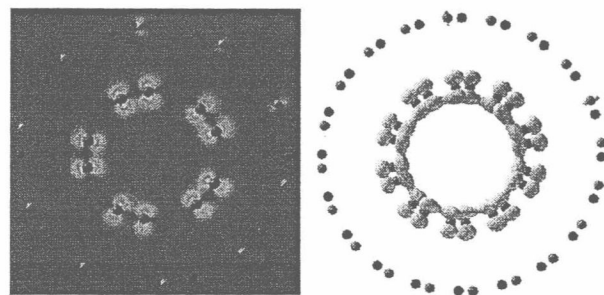

FIG. 3. (Color online) Charge density (left panel) and corresponding isosurface (right panel) of the conduction electrons on the two bands crossing the Fermi level. Red, green, and blue balls stand for carbon, nitrogen, and boron atoms, respectively. Red, yellow, green, and blue colors in the left panel represent the magnitude of electron density in descending order.
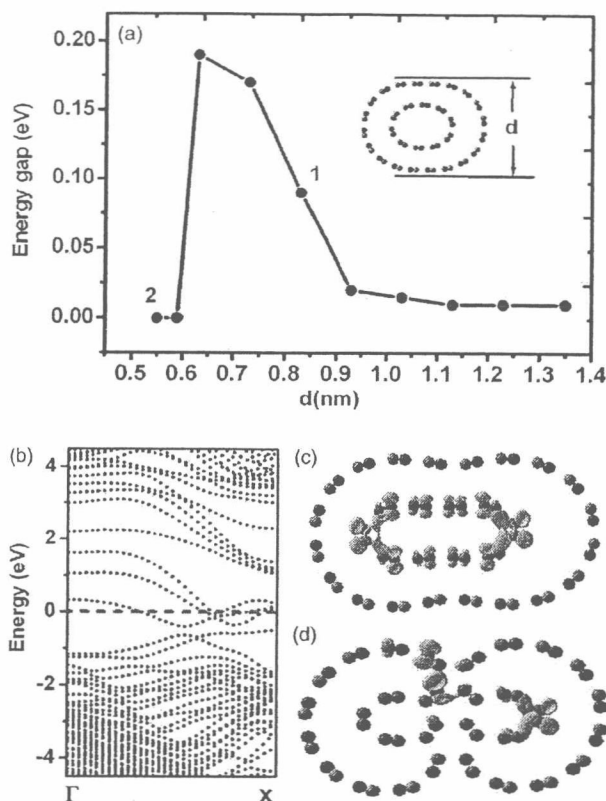
FIG. 4. (Color online) Behavior of the (5, 5)-(10, 10) nanocable under radial deformation. (a) The energy gap of the nanocable as a function of the distance between the two tips. (b) The electronic band of the nanocable under deformation at point labeled by 2 in (a). (c) and (d) are the isosurface of charge density of the bands crossing the Fermi level under deformation at points labeled by 1 and 2 in (a), respectively. The short dash line denotes the Fermi level in (b).

conductive capacity under the tensile deformation. In fact, the CNT can be modulated from semiconductor to metal by an axis-oriented magnetic field,[12] while the energy gap of the outer BNNT can hardly be changed by it. Thus the inner CNT is not necessary to be metallic initially. In addition, due to excellent dielectric properties and high resistance to penetration in bulk hexagonal BN, the transverse penetration voltage of the studied nanocable is expected to increase by at least 14 times when compared with that of bare CNT case. Multiwalled BNNTs should provide better antipenetrating properties.

In conclusion, our *ab initio* study on the coaxial nanocable consisting of a metallic CNT core and an insulating BNNT sheath shows that the BNNT can serve well as an insulating sheath while the CNT core possesses excellent transport ability, and the nanocable is robust enough to mechanical deformation. The excellent transport and mechanical properties of the proposed nanocable make it a potential in future nanodevices.

[1]H. G. Craighead, Science **290**, 1532 (2000).
[2]K. Suenaga, C. Colliex, and N. Demoncy, Science **278**, 653 (1997).
[3]Y. Zhang, K. Suenaga, and C. Colliex, Science **281**, 973 (1998).
[4]K. Suenaga, Y. Zhang, and S. Iijima, Appl. Phys. Lett. **76**, 1564 (2000).
[5]D. P. Yu, Y. J. Xing, and M. Tence, Physica E (Amsterdam) **15**, 1 (2002).
[6]Q. Li and C. R. Wang, Appl. Phys. Lett. **82**, 1398 (2003).
[7]H. Z. Zhang, X. H. Luo, and J. Xu, J. Phys. Chem. B **108**, 14866 (2004).
[8]J. C. Yu, X. L. Hu, and Q. Li, Chem. Commun. (Cambridge) **2005**, 2704 (2005).
[9]Z. Zhou, J. Zhao, and Z. Chen, C. R. Math. **110**, 2529 (2006).
[10]M. M. Treacy, T. W. Ebbesen, and J. N. Gibson, Nature (London) **381**, 678 (1996); E. W. Wong, P. E. Sheehan, and C. M. Lieber, Science **277**, 1971 (1997).
[11]W. L. Guo and Y. F. Guo, Phys. Rev. Lett. **91**, 115501 (2003).
[12]J. P. Lu, Phys. Rev. Lett. **74**, 1123 (1995).
[13]A. Rubio, J. L. Corkill, and M. L. Cohen, Phys. Rev. B **49**, 5081 (1994).
[14]D. Golberg, Y. Bando, and K. Kurashima, Solid State Commun. **116**, 1 (2000); D. Golberg, Y. Bando, and L. Bourgeois, Appl. Phys. Lett. **77**, 1979 (2000).
[15]W. Mickelson, S. Aloni, W. Q. Han, J. Cumings, and A. Zettl, Science **300**, 467 (2003); S. Okada, S. Saito, and A. Oshiyama, Phys. Rev. B **64**, 201303 (2001).
[16]A. Trave, F. J. Ribeiro, and S. G. Louie, Phys. Rev. B **70**, 205418 (2004).
[17]G. Kresse and J. Hafner, Phys. Rev. B **47**, 558 (1993); **49**, 14251 (1994); G. Kresse and J. Furthmuller, *ibid.* **54**, 11169 (1996).
[18]H. J. Xiang, Jinlong Yang, and J. G. Hou, Phys. Rev. B **68**, 035427 (2003).
[19]J. Q. Lu, J. Wu, and W. Duan, Phys. Rev. Lett. **90**, 156601 (2003).
[20]H. Mehrez, A. Svizhenko, and M. P. Anantram, Phys. Rev. B **71**, 155421 (2005).

formation of sp^3-type bonds and are considerably mixed with the states on BNNT, which suggests, in this case, that the charge transport would be both on the inner CNT and the outer BNNT. Nevertheless, the excellent conduction of the proposed nanocable is survived even when $d=0.83$ nm as the conduction electrons are still mainly concentrated on the inner CNT [Fig. 4(c)], which suggests that the nanocable can suffer a radial pressure up to 500 GPa. Therefore, the proposed nanocable is robust enough under radial deformation.

If other metallic-type CNTs are adopted as the inner core of the cable, we can infer that an excellent nanocable can also be obtained. In this case, the band gap of the CNT core will be varied under the uniaxial strain. Nevertheless, the variation is located within 0.1 eV even when the strain is up to 5%, while the outer BNNT is inert to stretching. Thus the proposed nanocable exhibits high robustness for convincing

Two Distinct Buckling Modes in Carbon Nanotube Bending

Xiaojie Duan,[†] Chun Tang,[‡] Jin Zhang,*[†] Wanlin Guo,*[‡] and Zhongfan Liu*[†]

Beijing National Laboratory for Molecular Sciences, Key Laboratory for the Physics and Chemistry of Nanodevices, Centre for Nanoscale Science and Technology, College of Chemistry and Molecular Engineering, Peking University, Beijing 100871, China, and Institute of Nano Science, Nanjing University of Aeronautics and Astronautics, Nanjing 210016, China

ABSTRACT

By using controlled SPM manipulation, carbon nanotubes have been continuously bent into a series of increasing angles, and two distinct buckling modes corresponding to "abrupt" and "gradual" buckle formation were observed through recording the height increment at the bend site during the loading process. Molecular dynamics simulation also found the two buckling modes in different types of carbon nanotubes, and their atomistic mechanism was revealed. Finally, the dependence of the critical buckling condition on diameters of carbon nanotubes was tentatively studied.

The buckling behavior is a fundamental mechanical property of carbon nanotubes (CNTs). It is found that the electrical conductance and the effective bending modulus of CNTs will be significantly changed by the formation of a buckle.[1,2] This makes a comprehensive understanding of the buckling occurrence such as the buckling mode and critical buckling condition important for future applications of CNTs in the nanoelectromechanical system (NEMS) and superstrong composite materials.[3,4] Compared to the abundant theoretical efforts concerning the buckling behavior of CNTs,[2,5−7] the direct experimental study is limited due to the small dimension of CNTs. Although the existence of the buckle in bent single- and double-walled carbon nanotubes[6] and the wavelike wrinkle in multiwalled carbon nanotubes (MWNTs)[8] has been determined by high-resolution transmission electron microscopy (HRTEM) and scanning probe microscopy (SPM),[9,10] the experimental report on the buckle formation process and critical buckling condition and their dependence on tube structures is still limited. The limitation mainly lies in the difficulty in controlled deforming of the carbon nanotubes.

In the present study, the structure evolution of individual carbon nanotubes in the bending process is systematically investigated through continuously bending the tubes to different angles by SPM manipulation. Measurements of the height change at the buckling site show two distinct buckling modes: the abrupt transition from uniform elastic bending to buckling at a critical bending angle accompanying a height jump and the gradual transition with the height increasing slowly. Using molecular dynamics (MD) simulations, the two buckling modes are consistently reproduced in different types of CNTs, and the atomistic mechanism of the two modes is revealed. Furthermore, a special "dual-size" effect concerning the important role of tubes thickness and diameter in determining their buckling modes was predicted. Finally, the dependence of the critical buckling condition on diameters of carbon nanotube was tentatively studied.

All carbon nanotubes used in our bending experiments were grown directly on silicon (111) surfaces with a 200 nm thick SiO_2 layer by chemical vapor deposition (CVD). Briefly, $Fe(OH)_3$ colloids hydrolyzed from $FeCl_3$ were spin-coated onto silicon surfaces to act as the catalysts, and the carbon nanotube growth was carried out at 775 °C for 5 min with a flow of ethene at 10 standard cubic centimeters per minute (sccm) and hydrogen and argon at 600 sccm, respectively. The carbon nanotubes prepared using this direct surface growth are free from defects and contamination of amorphous carbon.[11,12] The diameter of the as-grown carbon nanotubes is mainly in the range of 1−2 nm with a few exceptions. For the bending test, straight ends of carbon nanotubes with different diameters were purposely chosen. All carbon nanotubes here can be manipulated repeatedly without any cleavage. This proves that they are individual carbon nanotubes rather than bundles.

The SPM bending manipulation was conducted using a Nanoscope III SPM (Veeco) with specifically compiled software (see Supporting Information). Normally, the SPM

* Corresponding authors. E-mail: jinzhang@pku.edu.cn (J.Z.); zfliu@pku.edu.cn (Z.L.); wlguo@nuaa.edu.cn (W.G.).
† Peking University.
‡ Nanjing University of Aeronautics and Astronautics.
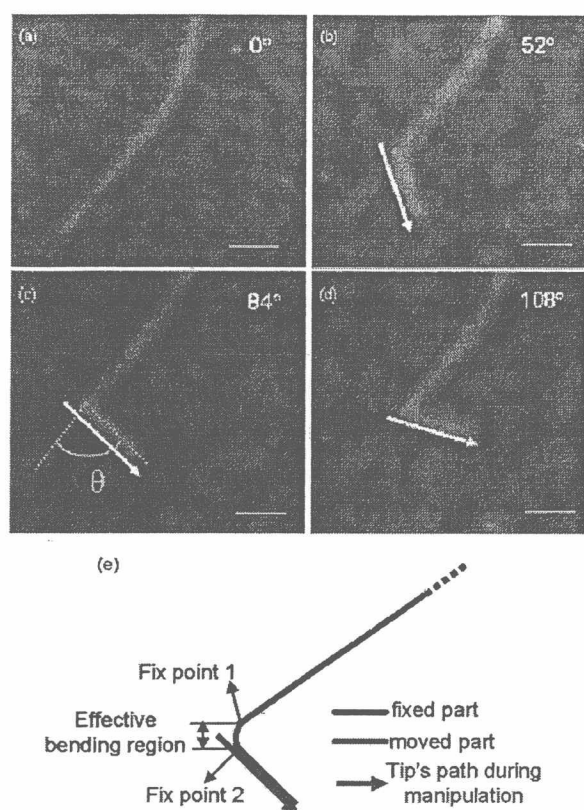
Figure 1. Tapping-mode AFM height images of a carbon nanotube bent to different angles. The angles between the initial and final position of the moved part was defined as the bending angle θ as shown in panel c. In the top right corner of each image, the bending angles are shown. During the manipulation, the end segment has been pushed along the path shown by the white arrows. The direction and position of the tube end segment was determined by the tip's path, which made it possible to control the bending angle. Scale bar: 50 nm. (e) Schematic figure of the detailed bending structure of carbon nanotubes. There is only vdW interaction between the substrate and the moved part indicated by the blue line.

was operated in tapping atomic force microscopy mode in air. For a typical bending manipulation, the tip was pressed down about 5−20 nm with the feedback switched off for an optimal contact load at the tip−sample interface. After that, the tip moved horizontally along a predefined straight path, which had a small angle with the axis of the end segment that would be manipulated (as shown by the white arrow in Figure 1) and pushed the end segment that had a typical length of about 100 nm. Then the tip returned to the normal imaging distance, and the feedback was switched on to get the images of the bent tubes.[13,14] All the height measurement from the AFM image was conducted with a linear fit of the substrate profile as captured, without plane fitting.[15] The diameter values were an average of more than 10 points along the tubes. Figure 1 shows typical bending results of a carbon nanotube with a diameter of 1.31 nm. It can be seen that the position and direction of the manipulated segment was definitely determined by the tip's path. In our system, because of the straight manipulation path, the main part of the moved segment was straight and the effective bending

segment was localized in a small region, which appeared as the cross point of the fixed and moved part due to the AFM resolution limitation.[16] We define the angle between the manipulated part and its initial position as the bending angle θ, which is closely related with the curvature of the effective bending region. By simply predefining the tip path during manipulation, the bending angle could be controlled, which made the observation of the structure evolution in the whole bending process possible. The bending configuration was maintained by the interaction between tubes and substrate.

Table a in Figure 2 shows the heights of the bend "point" at different bending angles of this tube. An increment in height was caused by the first manipulation to 26°. Actually, this elevation happened for the entire moved segment. This can be seen from the section analysis in Figure 2c: in the black profile, there was no difference in the height of the bend "point" and the straight moved part, while in the red profile, the height of the bend "point" was obviously larger than that of the fixed part. The elevation of the moved part caused by the first manipulation in fact occurred in all carbon nanotubes we manipulated. In the following manipulation, the straight manipulated part would remain at this elevated height all the time. For the bend "point", as long as the bending had not reached the critical buckling condition, this elevated height would also remain constant. This height increment may be caused by the interaction decrease between the substrate and the manipulated CNTs segment compared to that between the substrate and the as-grown CNTs, as proved by the smaller force (less pressing-down distance of tip) needed to achieve the following manipulation than the first manipulation. Because of the smaller interaction of substrate with the moved part than with the fixed part, the bending strain would propagate along the moved segment rather than the fixed segment, and the effective bending region would locate in the moved segment, which interacted with the substrate only by van der Waals (vdW) force. It has been proved that this vdW interaction had no significant influence on CNT buckling behavior, as discussed in the following text. The schematic figure of the detailed bending structure can be found in Figure 1e.

To take this elevation into account when studying CNT buckling behavior, for the ΔH (increment in height) values, except for the bending angle 0° where it had been set as 0, other values at the bend "point" for all CNTs in this paper were calculated by a comparison with the values after the first manipulation (an average of the bend "point" heights at all bending angles before buckling) rather than the initial heights. The plot of the ΔH vs the bending angles for the tube with a diameter of 1.31 nm is shown in panel (b) of Figure 2. After the first manipulation, the height remained nearly constant until reaching 96°. As opposed to the case at bending angle 26°, the height increase at 96° only happened at the bend "point" when an obvious protuberance appeared. This can also be seen from the 3-D AFM height images (Figure S1a, Supporting Information). The height jump suggested a transition from uniform elastic bending to buckling of CNTs happened at a certain bending stage between 84° and 96°. This is consistent with the theoretical
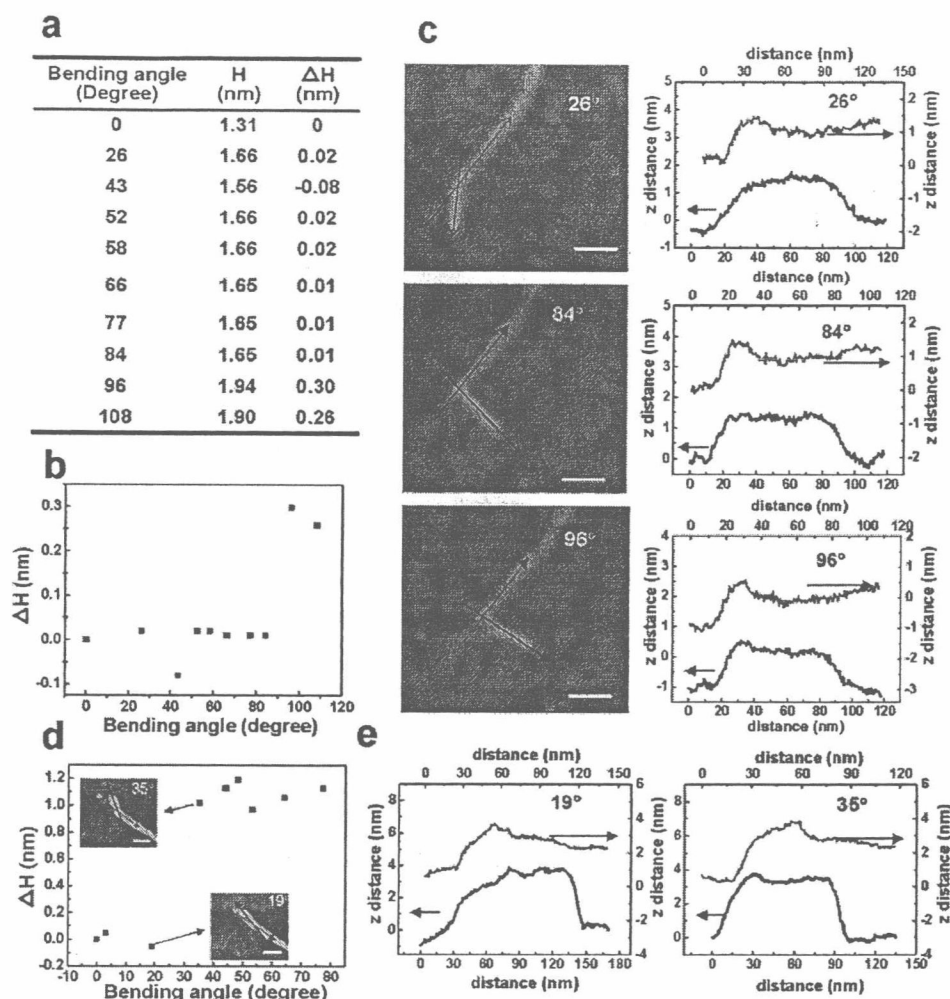
Figure 2. (a) Heights and height changes (ΔH) at the bend "point" of carbon nanotube with diameter of 1.31 nm at different bending angles. (b) Plot of ΔH vs bending angles. The red and black lines in the right panels of (c) correspond to the profiles marked with the red and black arrows in the left panels, respectively. In table a, because there was no height change before manipulation, the ΔH has been set as zero at 0°. All the following ΔH was obtained from a comparison with the average value of heights from 26° to 84° before buckling. (d) Plot of ΔH at the bend "point" of carbon nanotube with diameter of 3.17 nm vs bending angles. The insets are the AFM images of this tube at 19° and 35°. (e) Section analysis of tube with diameter of 3.17 nm at 19° and 35°. The red and black lines correspond to the profiles marked with the red and black arrows in the inset of d, respectively. All the scale bars in the AFM height images are 50 nm.

predictions: when the bending strain is small, the C−C bonds of CNTs have a slight stretch at the outer side of the bending region and a compression at the inner side, which appears as uniform elastic bending. This structure has no significant difference with straight tubes. When the strain is increased to a certain extent, a new pattern, buckling, would be formed accompanying a minimization of the strain energy.[5,6] This structure has a special atomic arrangement as compared to the normal carbon nanotubes. For this tube, this transition was abrupt and it caused a height increment of 0.28 nm (an average of the ΔH for all bending angles after buckling, same for the following tubes). In subsequent bending to 108°, the buckle structure was preserved with the height constant again. The result here observed the transition from uniform elastic bending to buckling of an individual carbon nanotube experimentally, and the critical buckling angle appeared to be in the range of 84−96° for this tube.

Another case is shown for a carbon nanotube with a diameter of 3.17 nm (Figures 2d,e and S1b, Supporting Information). When bent to 35°, the newly formed protuberance at the bend "point" indicated the occurrence of buckling. The critical buckling angle for this tube was therefore in the range of 19−35°, and the final ΔH corresponding to the buckle formation was 1.08 nm. We have designated this abrupt transition from uniform bending to a fully formed buckle, as exhibited by the above two tubes, "buckling mode I".

As opposed to the abrupt transition from uniform elastic bending to a fully formed buckle, some carbon nanotubes had another buckling behavior. Figure 3a,b shows the bending results for a carbon nanotube with a diameter of 2.82 nm. The difference lay in that, from 50° to 91°, the height had experienced a gradual increase before reaching the final constant value rather than an abrupt jump. From
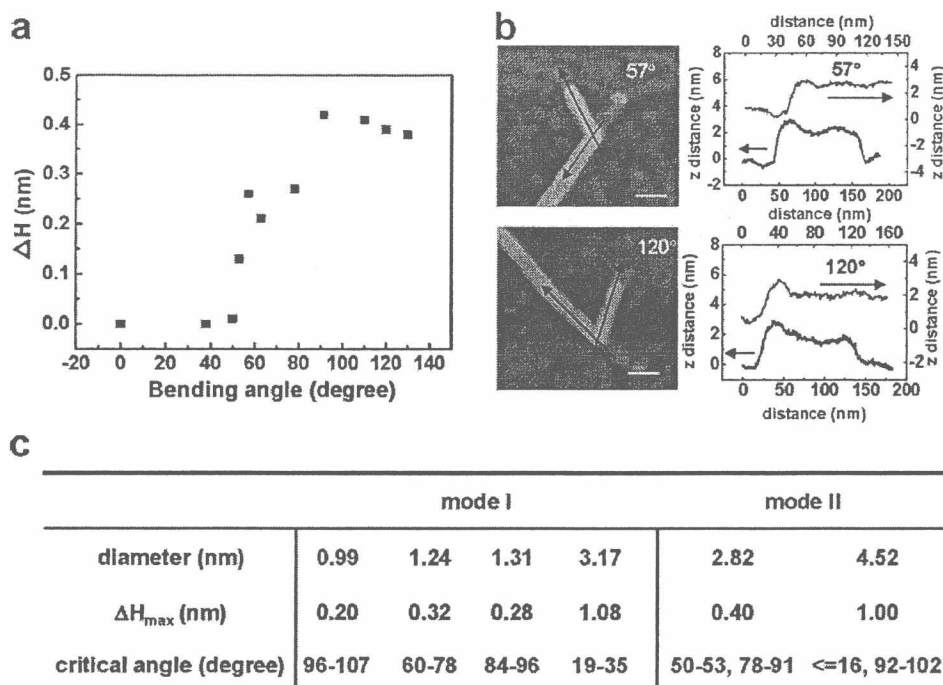
Figure 3. (a) Plot of ΔH at the bend "point" of carbon nanotube with diameter of 2.82 nm vs bending angles. It can be seen that there is a gradual increase in height from 50° to 91°. The red and black lines in the right panels of (b) correspond to the profiles marked with the red and black arrows in the left panels, respectively. From section analysis b and 3-D AFM height images (Figure S1c, Supporting Information), it can be seen that there is a small buckle formed at 57°, while at 120°, the buckle has been fully formed corresponding to the larger and stable protuberance at the bend site. All the scale bars in the AFM height images are 50 nm. Table c shows the critical buckling condition ranges and maximum height increment ΔH_{max} of different carbon nanotubes. For the two tubes of mode II, the first range is where the buckling begins and the second is where the buckling finishes.

the section analysis, it can be seen that, during this stage, for example at 57°, a small protuberance has been produced, while above 91°, the protuberance was larger and stable. The final maximum ΔH was 0.40 nm for this tube. This implied that the CNTs have experienced a series of intermediate states when transiting from the uniform elastic bending to the fully formed buckle. This was quite distinct from buckling mode I; we have designated this "buckling mode II".

By comparing the carbon nanotubes listed in table c of Figure 3, it was found that buckling mode I often happened for small-diameter CNTs, while mode II mainly occurred for larger-diameter tubes. To understand the atomistic mechanism of the two distinct buckling modes described above and also to explore their possible origin, molecular dynamics (MD) studies were conducted on CNTs of different types under bend loadings. In our MD simulations, the second-generation reactive empirical-bond-order potential was adopted. It was developed for hydrocarbons on the basis of the Tersoff—Brenner expression, and the L-J potential describing long-range vdW interaction was also included.[17,18] Three-walled, double-walled, and single-walled carbon nanotubes were modeled in this study. The bend loading was applied by giving a displacement of 0.2 Å to one end of the CNTs at each step, and then relaxing the whole system while keeping both ends of the CNTs fixed.

The two buckling modes were also observed by the simulations, and it was found that buckling mode I could be mainly observed in SWNTs, while buckling mode II mostly

occurred in MWNTs, which have thicker tube walls than SWNTs. Panel a in Figure 4 presented the ΔH with respect to the bending angles of the (9,9) SWNT, which has a diameter of 1.21 nm and a length of 24.5 nm. Before 39°, a small ΔH increase happened and the configuration of the bent tube had no significant change except for a slight ovalization of the cross section. This means that the SWNT underwent uniform elastic bending during this stage. Typical geometrical configuration was shown as the lower inset. At 41°, a sudden jump from 0.199 to 0.448 nm happened in ΔH, which corresponded to the abrupt transition from uniform elastic bending to buckling, as shown by the geometrical configuration in the upper inset. This phenomenon was qualitatively consistent with the experimental buckling mode I, and simulations on other SWNTs such as the (8,8), (17,0), and (14,14) SWNTs led to the same conclusion.

As for MWNTs, several double-walled and three-walled carbon nanotubes were modeled in our studies. Unlike SWNTs, all MWNTs in our simulations showed a gradual buckling process. As exampled by the (4,4)/(9,9)/(14,14) MWNT shown in Figure 4b, a gradual height increase happened that corresponded to a series of buckling intermediate states formation. Typical geometrical configurations at 23° and 30° were shown in the inset. It could be found that there was nearly no buckling for the inner layers, and the outer layers were partly buckling compared to the full buckling of corresponding tubular graphene layers in SWNTs.
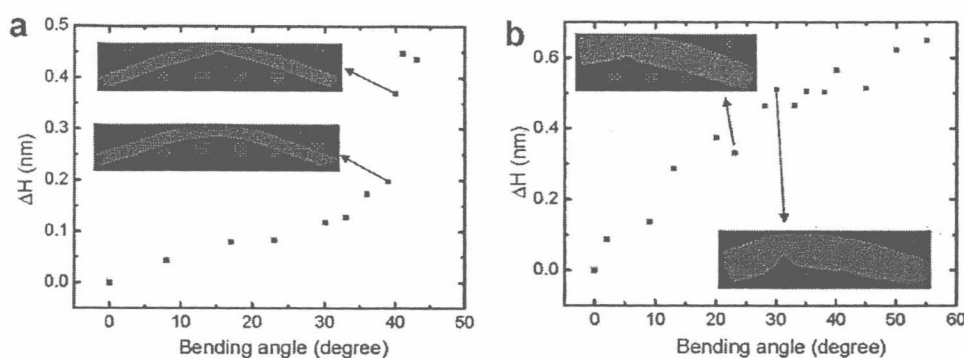
Figure 4. Molecular dynamics simulation results of carbon nanotubes under bend loadings. (a) Plot of ΔH vs bending angles of (9,9) SWNT, which is 1.21 nm in diameter and 24.5 nm in length. The sharp jump in ΔH can be observed from 39° to 41°. Insets are the representative geometrical configurations before (lower, 39°) and after (upper, 41°) buckling. (b) Plots of ΔH vs bending angles of (4,4)/ (9,9)/(14,14) MWNT, which is 1.9 nm in diameter and 12.2 nm in length; ΔH increases gradually during the whole process. Typical configurations of the intermediate buckling states are shown as the insets, which are under 23° and 30° bending, respectively.

Along with the increase of the bending angles, the buckling of all individual layers proceeded gradually. This was in agreement with the experimental results of buckling mode II.

The inhomogeneity of the buckling state between the inner and outer layers in MWNTs indicated the important role of thickness in tube-buckling behavior. As predicted by the theoretical studies, the critical buckling curvature of CNTs is closely related to their diameters (for example, it was found that, for SWNTs, the critical buckling curvature is inversely proportional to the square of tube diameter[5]). Thicker CNTs would have larger difference in inner and outer wall diameters. Thus at some bending stages, the outer wall would buckle first, while the inner walls remained stable. Furthermore, the radial elastic modulus of carbon nanotubes also increased with decreasing diameter.[19] The less-deformed inner tube would offer strong restraint to prevent the outer tube from dramatic deforming in transverse directions. Different layers buckled at different bending stages, and the partial buckling of outer layers operated together and resulted in the gradual buckling of MWNTs. Here, it can be seen that, for carbon nanotubes such a nanoscale object, the vdW interaction began to show significant influence on their mechanical property and made their buckling behavior distinct from the macroscopic shells. Furthermore, both the experiment and simulation indicated that special CNT structures may be developed during the bending process. This diversity of structures may have potential applications in future NEMS or other nanoelectronic devices.[3]

The thickness should not be the only factor influencing the CNT buckling behavior. Considering small-diameter SWNTs, although the interwall vdW does not exist, the vdW interaction between the inner and outer side of the bending from the same wall could become remarkable and may offer a restriction for the buckling. While if the diameters of MWNTs were large enough and their walls were not too thick, the difference in critical buckling conditions for the inner and outer walls may be negligible, so all the walls may buckle simultaneously and the inner tube would offer less constraint to hinder the outer tube's deformation. Their buckling behavior may be more like mode I. The above

analysis may explain the result of the tube that buckled as mode I while it had a diameter of 3.17 nm. So for the CNT buckling behavior, the thickness and diameter may have a cooperative effect. This cooperative effect has been proved by Chang et al. by using a molecular mechanics model.[7] The dependence of carbon nanotube properties on diameter could be regarded as a size effect, which is known as an important factor leading to special electronic, optical, magnetic, and chemical properties of nanomaterials.[20] Here, a special "dual-size" effect, diameter and thickness, which operated together to determine the CNT buckling behavior, may exist. This concept may be important for describing CNT mechanical properieties.

In a slightly different case from the isolated CNTs in simulation, there was vdW interaction between the substrate and the effective bending region of tubes in the experiment. However, by using molecular dynamics simulation, it has been proved that this vdW interaction had no significant influence on tube buckling (Supporting Information). That is why such a good agreement between experimental and theoretical results had been achieved.

By comparing the range of the critical angles of the four carbon nanotubes buckling as mode I in table c of Figure 3, it is found that the critical angles decreased along with the increase of the carbon nanotube diameters except those with diameters of 1.24 and 1.31 nm. The trend here was consistent with the theoretical predictions,[5] where an inverse relation between the critical buckling curvature and the square of carbon nanotube diameters has been proposed, although the clear relationship between the critical angles and diameters could not be deduced by far here. The deviation of the carbon nanotubes with diameters of 1.24 and 1.31 nm may arise from the influence of the helicity, which has also been theoretically predicted for carbon nanotubes less than 2.0 nm in diameter.[6] Note that the critical angles in this study from experimental observations are much larger than those in the MD simulations and that reported by Iijima et al.[6] The reason for the difference may be due to the larger length of the experimental effective bending region corresponding to the manipulation process here, which resulted in larger bending angles for the same curvature. For the carbon nanotubes